MARTIAN GEOLOGY

Organic synthesis associated with serpentinization and carbonation on early Mars

A. Steele[1]*, L. G. Benning[2,3], R. Wirth[2], A. Schreiber[2], T. Araki[4], F. M. McCubbin[5], M. D. Fries[5], L. R. Nittler[1], J. Wang[1], L. J. Hallis[6], P. G. Conrad[1], C. Conley[7], S. Vitale[1], A. C. O'Brien[6], V. Riggi[1], K. Rogers[8]

Water-rock interactions are relevant to planetary habitability, influencing mineralogical diversity and the production of organic molecules. We examine carbonates and silicates in the martian meteorite Allan Hills 84001 (ALH 84001), using colocated nanoscale analyses, to characterize the nature of water-rock reactions on early Mars. We find complex refractory organic material associated with mineral assemblages that formed by mineral carbonation and serpentinization reactions. The organic molecules are colocated with nanophase magnetite; both formed in situ during water-rock interactions on Mars. Two potentially distinct mechanisms of abiotic organic synthesis operated on early Mars during the late Noachian period (3.9 to 4.1 billion years ago).

The martian meteorite Allan Hills 84001 (ALH 84001) formed during the Noachian period on Mars: It has an igneous crystallization age of ~4.09 billion years (*1*–*3*). ALH 84001 is predominately composed of the silicate mineral orthopyroxene (hereafter Opx). It also contains carbonate globules (*3*) that have been linked to aqueous processes on early Mars ~3.9 billion years ago (*1*, *2*). As one of the oldest known rocks from Mars, ALH 84001 serves as a window into early planetary processes that may also have occurred on early Earth (*4*). Organic carbon, including possible nitrogen-containing organic compounds (*4*–*7*), has been described in ALH 84001. Hypotheses as to the provenance and formation mechanisms of these organics include abiotic production by impact-related (*8*), igneous (*6*), and/or hydrothermal processes (*5*, *7*); biological production by putative ancient martian organisms (*4*); and terrestrial contamination (*9*, *10*). To investigate the identity, origin, and formation mechanisms of organics, we applied colocated nanoscale spectral, imaging, structural, and isotopic analysis techniques to thin foils extracted from two subsamples of ALH 84001: the reported magnetite-rich crush zones of a thin section (designated ALH 84001,347) (*11*) and a cross-section through the center of a carbonate globule on a fresh fracture surface (designated ALH 84001,336) (*12*).

[1]Carnegie Institution for Science, Earth and Planets Laboratory, Washington, DC 20015, USA. [2]Deutsches GeoForschungsZentrum, Telegrafenberg, 14473 Potsdam, Germany. [3]Department of Earth Sciences, Free University of Berlin, 12249 Berlin, Germany. [4]Diamond Light Source, Harwell Science and Innovation Campus, Didcot OX11 0DE, UK. [5]NASA Johnson Space Center, Houston, TX 77058, USA. [6]School of Geographical and Earth Science, University of Glasgow, Glasgow G12 8QQ, UK. [7]NASA Ames Research Center, Mountain View, CA 94035, USA. [8]Earth and Environmental Sciences, Rensselaer Polytechnic Institute, Troy, NY 12180, USA.
*Corresponding author. Email: asteele@carnegiescience.edu

Colocated nanoscale analyses

We used a focused ion beam (FIB) to extract a foil (Fig. 1A) from an iron oxide–rich (magnetite) vein in a thin section of ALH 84001,347 (wider context shown in fig. S1C). Transmission electron microscopy (TEM) imaging of this foil shows that the Opx has a saw tooth or dentate appearance at its edge (Fig. 1, B and C); this is a characteristic feature of aqueous dissolution (*13*). The altered Opx surfaces are associated with a fibrous phase (labeled "1" in Fig. 1B) and an area of nanocrystalline material that is infilled with another fibrous phase (labeled "2" in Fig. 1C). Higher-resolution TEM images of the fibrous phases show that they are associated with nanocrystals of magnetite and carbonate (fig. S6B). Elemental compositional analyses of fibrous phases 1 and 2 show that their compositions are similar to those of lizardite and/or antigorite and to that of talc, respectively (Fig. 1D, table S1, and fig. S2). Bright-field TEM images of fibrous phases 1 and 2 (Fig. 1, E and G) indicate crystalline lattice fringes in an amorphous matrix with electron diffraction patterns (Fig. 1, F and H) exhibiting lattice *d*-spacings of ~9.6 Å and 9.2 to 9.7 Å (mean: 9.5 Å), respectively. These values correspond to basal plane distances of sheet silicates. We infer that both fibrous phases are predominately Fe-Mg silicates, containing a small amount of Al, with the appearance, chemical composition (Fig. 1D), and *d*-spacing characteristics of talc or possibly a serpentine subgroup mineral (Fig. 1D), hereafter referred to as a talc-like phase (*14*–*16*).

We obtained scanning transmission x-ray microscopy (STXM) spectral analysis of carbon (the C 1s edge) associated with the fibrous areas (Fig. 1I). These data indicate a range of organic functional groups colocalized with the fibrous phases (Fig. 1, B and C). The STXM peak distribution of these organics does not match potential contamination by the thin-section polymer used in ALH 84001,347 (table S2). The spectra indicate the presence of aromatic organic carbon (peak at 284.9 eV) and a range of organic oxygen functional groups, including carbonyl (286.5 eV), carboxyl (288.5 eV), and inorganic carbonate (290.4 eV). A small peak at 287.9 eV in spectrum 3 (asterisk in Fig. 1I) may be due to the presence of aliphatic or amidyl (C–NH) organic group functionality (spectrum 3 in Fig. 1I and table S2). We used nanoscale secondary ion mass spectrometry (NanoSIMS) to confirm the presence of carbon-rich material in the fibrous areas (Fig. 1J). Hydrogen isotopic analyses of these carbon-rich areas indicate that the organic matter and fibrous material are enriched in deuterium relative to Earth, with deuterium excess (δD) values of ~790 ± 140 per mil (‰) (Fig. 1K). This range of δD values differs from that of the thin-section polymer, which we measured to be ~−250 ± 50‰. The ALH 84001 data have a δD value within the range of the martian crustal H_2O reservoir, which is ~700 to 2700‰ (*17*). The high, positive δD values, combined with the multitude of organic carbon functional groups, indicate negligible contamination of the talc-like phase by the thin-section polymer.

We cut additional FIB sections across a carbonate globule from a fresh fracture surface of ALH 84001,336 to evaluate a portion of the meteorite that had not come into contact with the thin-section polymer (fig. S3). A FIB slice from the center of the carbonate globule reveals a denticular interface between the carbonate globule and Opx (Fig. 2, A to E, and fig. S2C), similar to that shown in Fig. 1. This Opx dissolution texture appears to have propagated along the (110) cleavage plane of Opx, perpendicular to (what appear to be) shock lamellae along the (100) plane (fig. S5). Chromite grains are present throughout the Opx (Fig. 2D). One such grain appears to have resisted the alteration process of the Opx as it protrudes from Opx into the carbonate (Fig. 2D). In addition to alteration at the Opx-globule interface, the FIB slice revealed a carbonate vein within the Opx that is contiguous with the globule (Fig. 2B). The carbonate within the vein and the globule appears to be zoned in a similar way to that described previously (*18*), with voids throughout its structure that contain single magnetite or siderite nanocrystals (fig. S4). A bright-field TEM image of the Opx-globule interface is nanocrystalline in appearance (Fig. 2E) and filled with an amorphous silicate, which we identified by means of energy-dispersive x-ray spectroscopy analyses and by a lack of lattice fringes in high-resolution TEM imaging (Fig. 2F and fig. S6). STXM analysis of this material (Fig. 2G) shows peaks corresponding to aromatic/olefinic carbon, as well as carbonyl, carboxyl, and carbonate groups (table S2). The carbonate peak at 290.4 eV dominates these spectra, but lower-energy organic carbon peaks are also present (Fig. 2G).

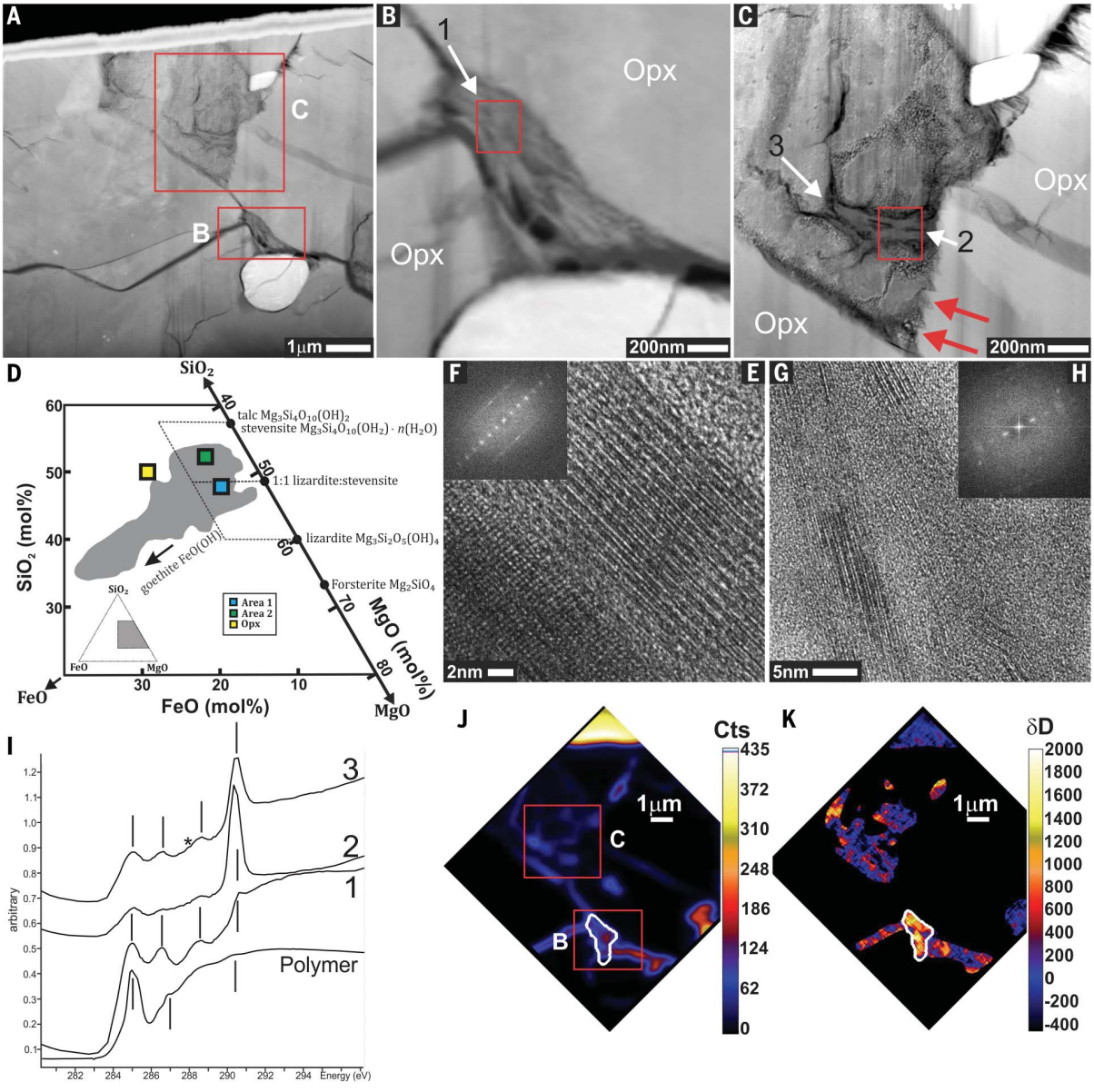

Fig. 1. Analysis of FIB foil taken from the ALH 84001 matrix. (**A**) Overview image of the foil; wider context is shown in fig. S1C. Red boxes outline the areas depicted in (B) and (C). (**B**) High-angle annular dark-field (HAADF) TEM image showing a fibrous phase infilling a crack between two slightly weathered Opx grains (arrow labeled "1"). The red box indicates area of analyses depicted in (E). (**C**) TEM HAADF image of microcrystalline material (white arrow labeled "3") infilled with a fibrous material (white arrow labeled "2"). The red arrows indicate areas of denticle formation from pyroxene dissolution, and the red box marks the area of analyses depicted in (G). (**D**) Truncated portion of a MgO-SiO_2-FeO ternary diagram, which shows the MgO, FeO, and SiO_2 molar abundances measured by energy-dispersive x-ray spectroscopy in areas 1 and 2 and host Opx [from white arrows in (B) and (C)] compared to those of serpentines from Oman (gray shaded region) (*14*). The inset shows the location of the truncated area in gray (see fig. S2B for a full ternary diagram). (**E**) TEM image of crystallites from the area within the red box in (B), showing lattice fringes indicative of a sheet silicate. (**F**) Fast Fourier transform (FFT) diffraction pattern of (E). (**G** and **H**) Same as (E) and (F) but for the area within the red box in (C). (**I**) STXM spectra from areas labeled with white arrows 1 to 3 in (B) and (C) compared with the spectrum for a thin-section polymer within the sample. Black vertical lines represent peak centers of interest; the asterisk denotes a small shoulder peak (see main text for details). (**J**) NanoSIMS map of ^{12}C abundance (Cts, counts); the red boxes indicate the fibrous material depicted in (B) and (C). (**K**) Same as (J) but for H isotopic analysis. The area outlined in white corresponds to the fibrous material in (B) and has δD = 790 ± 140‰.

Figure 2H shows a STXM map of the carbonate peak (at 290 eV) in the area of Opx dissolution textures shown in Fig. 2D, and the locations from which STXM spectra were collected are shown in Fig. 2, E and H. Hydrogen isotopic analysis of the organic carbon, measured in the same area as the STXM analysis (Fig. 2J), indicates that δD = 850 ± 400‰, within the range of values for the martian crust (*17*).

Analysis of a third FIB section (Fig. 3), taken from the rim of the same carbonate globule (Fig. 2), revealed a chaotic interface between carbonate, Opx, and a magnetite- and pyrite-rich rim material (RimM) that occurs at the edge and at the base of the globule (Fig. 3B). A second veinlike feature that cuts across the Opx contains rim material that transitions into a carbonate vein that is contiguous with

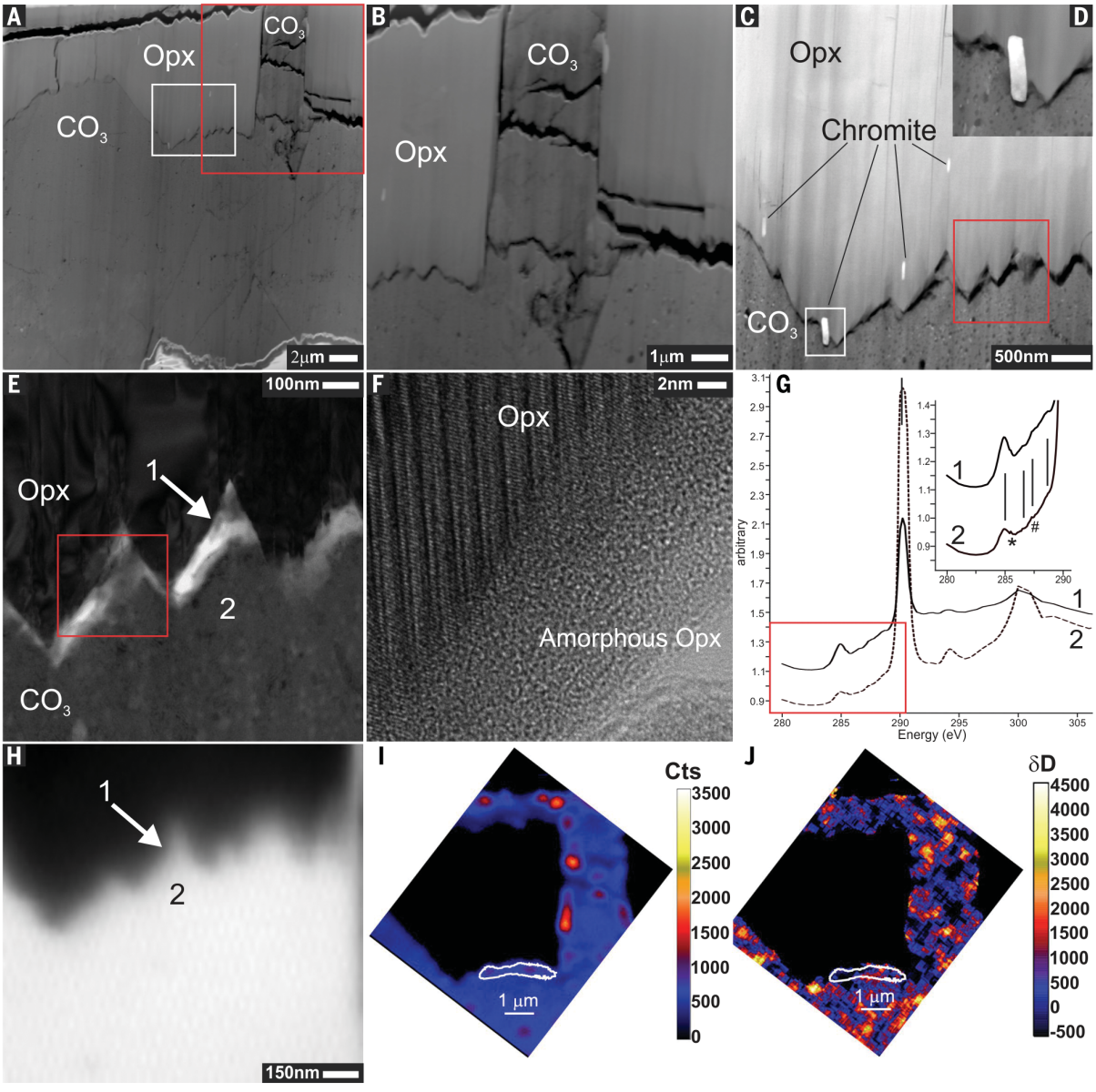

Fig. 2. Analysis of FIB foil taken from the center of a carbonate globule from ALH 84001. (**A**) TEM HAADF image of a slice through the center of the globule. The red box indicates the area shown in (B); the white box indicates the area depicted in (C) and (D). Broader context is shown in fig. S3. (**B**) Zoomed-in HAADF image [from red box in (A)] showing a carbonate vein connected to the carbonate globule. (**C**) HAADF image zoomed in on the carbonate-pyroxene contact; multiple small chromite grains oriented along the 110 axis of Opx are visible. The Opx exhibits denticular texture indicative of aqueous weathering. The white box surrounds a small chromite grain [magnified in (D)], and the red box shows a denticular area of Opx [magnified in (E)]. (**D**) Close-up image of a chromite grain [from (C)] protruding into the carbonate from the pyroxene. (**E**) TEM bright-field image of the carbonate-pyroxene contact shown in (C). The red box indicates the approximate area shown in (F). (**F**) TEM lattice fringe image of the crystalline-amorphous Opx interface, as indicated by the presence of lattice fringes and an amorphous material between the carbonate and the pyroxene. (**G**) STXM spectra of regions 1 and 2 from (E) and (H). The black lines indicate major peaks, the asterisk denotes a small shoulder peak, and the # symbol indicates a possible artefact peak. The inset is a magnified view of the region within the red box. (**H**) STXM map of the carbonate peak at 290 eV of the same denticular area as that shown in the red box in (C). The locations of STXM spectra 1 and 2 are indicated. (**I**) NanoSIMS ^{12}C map of the carbonate vein shown in (B) and (C). The area outlined in white corresponds to the Opx-carbonate contact in the same region as that depicted in (C) and (E). (**J**) NanoSIMS δD map of the same area as depicted in (I). For the organic-rich areas measured within the region outlined in white, we measured a δD of 850 ± 400‰.

the globule (Fig. 3, B and C). A bright-field TEM image of the rim material (Fig. 3D) shows a nanocrystalline mixture of phases infilling the space between the Opx denticles. A single nanocrystal of magnetite (~5 nm in diameter; Fig. 3, E and F) is surrounded by an amorphous material composed mainly of silica (fig. S7). The C 1s STXM spectra of five different locations within the RimM material (Fig. 3H) reveal the presence of carbonate and organic carbon that exhibit a functionality distribution similar to that observed in the areas depicted in Figs. 1 and 2 (see also Fig. 3H and table S2). NanoSIMS analysis of ^{12}C and δD in this organic material (Fig. 3, I and J) also shows elevated δD values (400 ± 170‰) that are between those of the martian crust and depleted martian mantle (*17*).

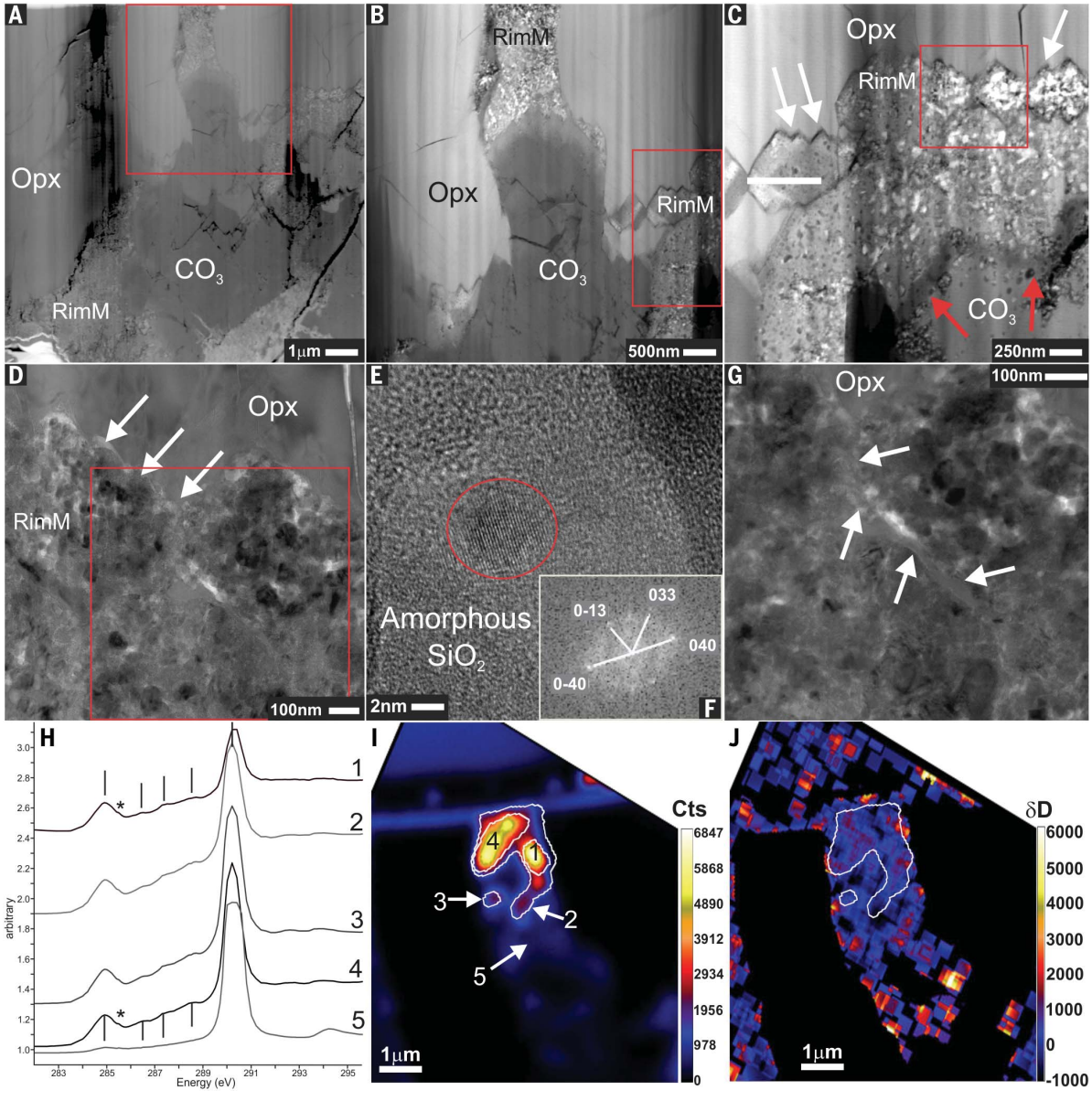

Fig. 3. Analysis of FIB foil taken from the rim of a carbonate globule from ALH 84001. The carbonate globule is the same as that shown in Fig. 2. (**A**) TEM HAADF image of a FIB section taken from the rim area of the globule shown in fig. S3 (the top of the globule is at the bottom of the image). The red box indicates the area shown in (B) and approximates the areas shown in (I) and (J). (**B**) TEM HAADF image of a vein of CO_3 and RimM material at the base of the carbonate globule. Rim material can also be observed underneath the carbonate at the pyroxene-carbonate interface, indicated by the red box, which is shown in more detail in (C). (**C**) Close-up view of the rim material at the interface between Opx and the CO_3 globule. White arrows denote the denticular boundary of the pyroxene edge; red arrows indicate a chevron-like contact between the carbonate and the RimM that we interpret as an area of transition or alteration between the pyroxene and carbonate. The red box denotes the area shown in (D). (**D**) Bright-field image of the area outlined by the red box in (C), revealing the contact of RimM and the CO_3 globule. The lighter areas in this image are holes or pores in the sample. White arrows indicate the boundary between Opx and RimM material. (**E**) TEM lattice fringe image of amorphous silica vein from (D) and (G), revealing a single magnetite grain (outlined by red ellipse) within a matrix of amorphous silica (marked as amorphous SiO_2). (**F**) FFT diffraction pattern of the magnetite grain in (E) [white arrows and text represent Miller indices (*hkl*)]. (**G**) Bright-field TEM image of the area outlined by the red box in (D). White arrows point to an amorphous silica vein that runs through RimM. (**H**) STXM spectra from spots taken within RimM and carbonate, showing differences in the amount of included organic matter within carbonate. Numbers indicate spectra taken from the areas shown in (I). The black vertical lines indicate major peaks; the asterisk denotes a small shoulder peak. (**I**) ^{12}C NanoSIMS map of the carbonate vein in (A) [approximate area shown is enclosed within the red box in (A)], depicting bright spots of organic material within carbonate. Numbers correspond to the spectra in (H). (**J**) δD map of the same area as in (I). The organic material within the white contour has δD = 400 ± 170‰.

Implications for early Mars

The microdenticular texture of Opx that we observe in ALH 84001 indicates aqueous and/or hydrothermal alteration of Opx, consistent with previous interpretations (*13*, *18*). The carbonate, amorphous silicate, and hydrated silicate phases that formed during alteration of ALH 84001 are not volumetrically dominant, indicating that fluid-rock reactions were not active for a prolonged time period. However, the phase assemblages that occur at the outer edges of the altered Opx (i.e., amorphous

silica; talc-like phases; magnetite; and predominately Fe-, Mg-, and Ca-rich carbonates) are similar to those observed in rocks from Earth that have undergone serpentinization and/or mineral carbonation, which indicates that similar alteration processes operated on early Mars. Whether the hydration and carbonation processes occurred as part of a single metasomatic event or as distinct events remains unclear. Previous work has suggested that ALH 84001 may have undergone more than one fluid event, possibly associated with pre-ejection impact events that caused the formation of crush zones in ALH 84001 (*11*, *19*, *20*). Formation of serpentinites on Earth requires a balance of many variables (*14*), including host rock composition (*21*), temperature, pressure, pH, silica activity, anion and cation concentrations, reduction and oxidation, water activity in the fluid phase, and partial pressure of CO_2 (*22*–*25*). This balance can produce a diverse mix of talc- or serpentine-like mineral phases during aqueous and/or hydrothermal alteration (*14*, *21*–*25*), making it difficult to constrain the conditions of fluid composition or the formation temperature for the alteration phases in ALH 84001, particularly given the later influence of impact ejection (*12*). Consequently, we cannot determine the timing or formation mechanisms of the talc, carbonate, and organics, but the simplest explanation is that these materials are reaction products of the interaction of Opx with hydrothermal fluid(s) of neutral to high pH (*22*). Our observations of Opx corrosion, the colocation of organic carbon and nanophase magnetite, and the alteration mineral assemblage(s) lead us to conclude that serpentinization and carbonation reactions occurred on Mars in the late Noachian and were a source of endogenous martian organic carbon.

Organic synthesis

Serpentinization is an abiotic organic synthesis mechanism whereby basaltic rocks react with an aqueous fluid, producing serpentine minerals, magnetite, and hydrogen (*26*, *27*). The hydrogen produced in this reaction is then available to reduce aqueous CO_2 to methane (via the Sabatier reaction or the reverse water-shift reaction) as well as to CO and other organics such as formic acid and formaldehyde (*26*–*29*). CO and H can also react via Fischer-Tropsch–type reactions to produce alkanes and other organic molecules, including nitrogen-containing organics (*29*, *30*). In ALH 84001, organics are colocated with magnetite in two different mineral assemblages. In the portion of the sample shown in Fig. 1, the magnetite coexists with a talc-like phase, indicating that martian serpentinization reactions are responsible for the formation of the observed organic compounds. By contrast, portions of the sample depicted in Figs. 2 and 3 show the presence of magnetite within an area containing only amorphous silica, carbonate, and organic carbon, indicating that martian mineral carbonation reactions are also responsible for the formation of organics. We did not detect organic material in cracks or fissures outside of those mineral assemblages; therefore, we discount external sources of organic material formed or transported into the sample from elsewhere on Mars. Previous studies have suggested biogenic processes (*4*), thermal decomposition of siderite (*8*), and/or aqueous abiotic hydrothermal processes (*5*, *7*) for the origin of organics in ALH 84001. Our results indicate that the deuterium-rich organic material is associated with the precipitation of nanophase magnetites in the presence of silica and carbonate (akin to mineral carbonation) and in the presence of talc-like phases (akin to serpentinization), consistent with aqueous abiotic hydrothermal processes (*26*–*29*). The organic material is aromatic and associated with carbonyl, carboxyl, and carbonate group functionality; similar features have been observed to be spatially correlated with mineral catalysts in other martian meteorites (e.g., Tissint, Nakhla, and NWA 1950) (*31*). Similar refractory aromatic organic material has also been detected through in situ analyses facilitated by the Curiosity rover (*32*).

Martian habitability

We conclude that aqueous alteration of the Opx in ALH 84001 caused the formation of carbonate globules, amorphous silicates and silica, and talc-like phases. This phase assemblage indicates that serpentinization and mineral carbonation reactions took place on early Mars, consistent with orbital observations of serpentinized terrains on Mars and studies of the martian meteorite Nakhla (*33*–*35*). Serpentinization and mineral carbonation reactions occur by aqueous alteration of mafic igneous mineral assemblages by CO_2-bearing fluids. Organic synthesis in ALH 84001 proceeded in a manner similar to serpentinization of rocks from Earth, producing aromatic, aliphatic, carbonyl, carboxyl, and carbonate species from aqueous CO_2. The correlation of organic material with both serpentinization and carbonation assemblages indicates that abiotic organic synthesis can occur from both reactions. The similarity of the organics in the ~4.0-billion-year-old ALH 84001 and those found in the ~600-million-year-old Tissint meteorite (*31*) indicate that Mars hosted abiotic organic synthesis reactions for much of its history. On Earth, these reactions are responsible for abiotic organic synthesis, methane production, and mineralogical diversity (*29*). On Mars, such reactions are relevant to habitability and have been invoked to explain the presence of methane in the atmosphere (*36*).

REFERENCES AND NOTES

1. L. E. Borg *et al*., *Science* **286**, 90–94 (1999).
2. T. J. Lapen *et al*., *Science* **328**, 347–351 (2010).
3. D. W. Mittlefehldt, *Meteoritics* **29**, 214–221 (1994).
4. D. S. McKay *et al*., *Science* **273**, 924–930 (1996).
5. A. Steele *et al*., *Meteorit. Planet. Sci.* **42**, 1549–1566 (2007).
6. A. Steele *et al*., *Science* **337**, 212–215 (2012).
7. M. Koike *et al*., *Nat. Commun.* **11**, 1988 (2020).
8. A. H. Treiman, *Astrobiology* **3**, 369–392 (2003).
9. T. Stephan, E. K. Jessberger, C. H. Heiss, D. Rost, *Meteorit. Planet. Sci.* **38**, 109–116 (2003).
10. A. Steele *et al*., *Meteorit. Planet. Sci.* **35**, 237–241 (2000).
11. A. H. Treiman, *Meteoritics* **30**, 294–302 (1995).
12. Materials and methods and supplementary text are available as supplementary materials.
13. C. M. Phillips-Lander, C. Legett, A. S. Elwood Madden, M. E. Elwood Madden, *Am. Mineral.* **102**, 1915–1921 (2017).
14. J. C. de Obeso, P. B. Kelemen, *Philos. Trans. R. Soc. A* **378**, 20180433 (2020).
15. D. B. Nahon, F. Colin, *Am. J. Sci.* **282**, 1232–1243 (1982).
16. E. J. W. Whittaker, J. Zussman, *Mineral. Mag. J. Mineral. Soc.* **31**, 107–126 (1956).
17. J. J. Barnes *et al*., *Nat. Geosci.* **13**, 260–264 (2020).
18. K. L. Thomas-Keprta, S. J. Clemett, D. S. McKay, E. K. Gibson, S. J. Wentworth, *Geochim. Cosmochim. Acta* **73**, 6631–6677 (2009).
19. C. M. Corrigan, R. P. Harvey, *Meteorit. Planet. Sci.* **39**, 17–30 (2004).
20. J. M. Eiler, J. W. Valley, C. M. Graham, J. Fournelle, *Geochim. Cosmochim. Acta* **66**, 1285–1303 (2002).
21. B. W. Evans, *J. Petrol.* **49**, 1873–1887 (2008).
22. A. N. Paukert, J. M. Matter, P. B. Kelemen, E. L. Shock, J. R. Havig, *Chem. Geol.* **330–331**, 86–100 (2012).
23. L. E. Mayhew, E. T. Ellison, T. M. McCollom, T. P. Trainor, A. S. Templeton, *Nat. Geosci.* **6**, 478–484 (2013).
24. D. Daval *et al*., *Geochim. Cosmochim. Acta* **74**, 2615–2633 (2010).
25. C. Boschi, A. Dini, L. Dallai, G. Ruggieri, G. Gianelli, *Chem. Geol.* **265**, 209–226 (2009).
26. N. G. Grozeva, F. Klein, J. S. Seewald, S. P. Sylva, *Philos. Trans. R. Soc. A* **378**, 20180431 (2020).
27. T. M. McCollom, J. S. Seewald, *Chem. Rev.* **107**, 382–401 (2007).
28. B. Sherwood Lollar, T. D. Westgate, J. A. Ward, G. F. Slater, G. Lacrampe-Couloume, *Nature* **416**, 522–524 (2002).
29. N. G. Holm, A. Neubeck, *Geochem. Trans.* **10**, 9 (2009).
30. M. Schulte, E. Shock, *Meteorit. Planet. Sci.* **39**, 1577–1590 (2004).
31. A. Steele *et al*., *Sci. Adv.* **4**, eaat5118 (2018).
32. J. L. Eigenbrode *et al*., *Science* **360**, 1096–1101 (2018).
33. C. E. Viviano, J. E. Moersch, H. Y. McSween, *J. Geophys. Res. Planets* **118**, 1858–1872 (2013).
34. B. L. Ehlmann, J. F. Mustard, S. L. Murchie, *Geophys. Res. Lett.* **37**, L06201 (2010).
35. T. Tomkinson, M. R. Lee, D. F. Mark, C. L. Smith, *Nat. Commun.* **4**, 2662 (2013).
36. J. R. Lyons, C. Manning, F. Nimmo, *Geophys. Res. Lett.* **32**, L13201 (2005).
37. A. Steele *et al*., Data for "Organic synthesis associated with serpentinization and carbonation on early Mars," Dryad (2021); https://doi.org/10.5061/dryad.c2fqz6198.

ACKNOWLEDGMENTS

We thank A. Treiman, C. Boschi, and three anonymous reviewers for helpful comments during the preparation of this manuscript. We also thank the Meteorite Working Group, now the Antarctic Meteorite Review Panel of the Astromaterials Allocation Review Board, for carefully evaluating our sample requests and the curatorial staff at NASA Johnson Space Center for allocation of the ALH 84001 samples used in this study. The US Antarctic meteorite samples were recovered by the Antarctic Search for Meteorites (ANSMET) program, which has been funded by NSF and NASA and characterized and curated by the Department of Mineral Sciences of the Smithsonian Institution and the Astromaterials Acquisition and Curation Office at NASA Johnson Space Center, respectively. A.St., L.G.B., L.J.H., and A.C.O. thank Diamond Light Source for beam time (run MG2444) and acknowledge the input and help of B. Kaulich and M. Kazemian. **Funding:** A.St. acknowledges NASA grant 17-NAI8_2-0020 (principal investigator K.R.) and M. Walter (EPL) for travel funding. L.G.B., R.W., and A.St. acknowledge financial support for the TEM work through the Helmholtz Recruiting Initiative program awarded to L.G.B. F.M.M. acknowledges support from NASA's Planetary Science Research Program. **Author contributions:** A.St. collected data, performed data analysis, led the study, and led the writing of the paper. L.G.B., T.A., S.V., R.W., A.Sc., L.R.N., J.W., L.J.H., F.M.M., and A.C.O. performed data collection and analysis. F.M.M., M.D.F., P.G.C., C.C., V.R., and K.R. discussed

the interpretation of results and contributed to the writing of the paper. **Competing interests:** There are no competing interests to report for any of the authors. **Data and materials availability:** The main mass of ALH 84001 is stored at NASA Johnson Space Center, which makes samples available for research via https://curator.jsc.nasa.gov/antmet/requests.cfm?section=general. The FIB films we used are archived at the Carnegie Institution of Washington. See (*12*) for further details. Our microscopy, spectroscopy, and NanoSIMS data are archived at Dryad (*37*).

SUPPLEMENTARY MATERIALS

science.org/doi/10.1126/science.abg7905
Materials and Methods
Supplementary Text
Figs. S1 to S7
Tables S1 and S2
References (*38*–*60*)

2 February 2021; accepted 17 November 2021
10.1126/science.abg7905

Organic synthesis associated with serpentinization and carbonation on early Mars

A. SteeleL. G. BenningR. WirthA. SchreiberT. ArakiF. M. McCubbinM. D. FriesL. R. NittlerJ. WangL. J. HallisP. G. ConradC. ConleyS. VitaleA. C. O'BrienV. RiggiK. Rogers

Science, 375 (6577),

Abiotic formation of organic molecules

Mars rovers have found complex organic molecules in the ancient rocks exposed on the planet's surface and methane in the modern atmosphere. It is unclear what processes produced these organics, with proposals including both biotic and abiotic sources. Steele *et al*. analyzed the nanoscale mineralogy of the Mars meteorite ALH 84001 and found evidence of organic synthesis driven by serpentinization and carbonation reactions that occurred during the aqueous alteration of basalt rock by hydrothermal fluids. The results demonstrate that abiotic production of organic molecules operated on Mars 4 billion years ago. —KTS

Science (ISSN) is published by the American Association for the Advancement of Science. 1200 New York Avenue NW, Washington, DC 20005. The title *Science* is a registered trademark of AAAS.